Giant Nonlinear Response at the Nanoscale Driven by Bound States in the Continuum

Luca Carletti,[1] Kirill Koshelev,[2,3] Costantino De Angelis,[1] and Yuri Kivshar[2,3]
[1]Department of Information Engineering, University of Brescia, INO-CNR Via Branze 38/45, 25123 Brescia, Italy
[2]Nonlinear Physics Centre, Australian National University, Canberra ACT 2601, Australia
[3]ITMO University, St. Petersburg 197101, Russia

(Received 18 December 2017; published 19 July 2018)

Being motivated by the recent prediction of high-Q modes in subwavelength dielectric resonators inspired by bound states in the continuum (BIC), we study the second-harmonic generation from isolated subwavelength AlGaAs nanoantennas. We reveal that nonlinear effects at the nanoscale can be enhanced dramatically provided the resonator parameters are tuned to the BIC regime. We predict a record-high conversion efficiency for nanoscale resonators that exceeds by 2 orders of magnitude the conversion efficiency observed at the magnetic dipole Mie resonance, thus opening the way for highly efficient nonlinear metasurfaces and metadevices.

DOI: 10.1103/PhysRevLett.121.033903

Metaoptics governed by Mie-resonant nanoparticles has emerged recently as a new direction in nanophotonics [1], and it is expected to complement different functionalities of plasmonic structures in a range of potential applications [2]. All-dielectric nanoresonators have many advantages, including low losses and low heat dissipation, that can make them efficient building blocks for novel photonic metadevices. Importantly, the coexistence of strong electric and magnetic Mie-type resonances can result in constructive or destructive interferences with unusual beam shaping, or lead to resonant enhancement of magnetic fields in dielectric nanoparticles that can bring many novel effects in the nonlinear regime [1].

Low-order Mie resonances are known to exhibit relatively low values of quality factors (Q factors) [2]. Nevertheless, recently it was revealed [3] that subwavelength nanoscale resonators can support localized states with high Q factors provided their parameters are closely matched to the bound states in the continuum (BIC) [4] formed via destructive interference of two similar leaky modes [5,6]. A true BIC is a mathematical abstraction since its realization demands infinite size of the structure or zero or infinite permittivity [7,8]. Nevertheless, high-index dielectric nanoparticles can exhibit high-Q resonances via a BIC-inspired mechanism associated with the so-called supercavity modes [9].

The important questions are if those large Q factors can enhance nonlinear effects at the nanoscale [10,11] and how large this enhancement can be. Nonlinear optics at the nanoscale is governed by strong field confinement and resonances [10], and is not hampered by phase matching [12]. The field localization in dielectric nanoparticles is expected to occur near electric and magnetic Mie resonances that can be largely tuned in frequency by their geometric parameters [1].

In this Letter, we study second-harmonic generation (SHG) from isolated subwavelength nanoantennas, as presented schematically in Fig. 1. We predict a giant enhancement of nonlinear effects provided the resonator parameters are tuned to the BIC regime. The predicted record-high conversion efficiency exceeds by 2 orders of magnitude the largest conversion efficiency at the nanoscale demonstrated so far, opening up the door for many important applications of nonlinear and quantum nanophotonics.

Before presenting our main results, we notice that it is customary to define the SHG efficiency as $\gamma_{\mathrm{SH}} = P_{\mathrm{SH}}/P_{\mathrm{FF}}^2$, where P_{SH} is the total radiated power at second harmonic (SH) and P_{FF} is the pump power incident on the resonator at the fundamental frequency (FF). As defined by this relation, SHG conversion efficiencies in plasmonic nanoantennas up to 5×10^{-10} W^{-1} have been demonstrated [13–15]. An important improvement was recently possible for dielectric nanoantennas where $\gamma_{\mathrm{SH}} \sim 10^{-6}$ W^{-1} was demonstrated [16–19] near multipolar resonances.

However, the proposed definition of SHG efficiency does not take into account that only a percentage of the pump power is actually coupled to the cavity mode. To take this issue into account, we define an *intrinsic conversion efficiency* ρ_{SH} independent of the shape of the pump beam,

$$\rho_{\mathrm{SH}} = \frac{\gamma_{\mathrm{SH}}}{\eta^2} = \frac{P_{\mathrm{SH}}}{(\eta I_m A)^2}, \tag{1}$$

where I_m is the pump power density impinging on the resonator, and A is the geometrical cross section of the resonator. The term η is the coupling coefficient between the pump beam and the resonator mode at the pump frequency. For resonator modes with Q factors of more than 10, their electromagnetic field is indistinguishable to

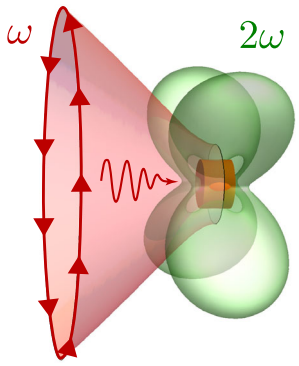

FIG. 1. Artistic view of the second-harmonic field generated from a subwavelength dielectric nanoparticle pumped by an azimuthally polarized beam at the BIC conditions.

the profile of modes of the closed cavity since the radiation losses can be treated as a weak perturbation. Therefore, η can be defined as the spatial overlap integral between the electric fields of the pump beam, E_p, and the resonator mode, E_c, at the upper resonator surface A:

$$\eta = \frac{|\int_A E_p^* E_c dS|^2}{(\int_A |E_p|^2 dS)(\int_A |E_c|^2 dS)}. \quad (2)$$

Thus, the enhancement of extrinsic SHG conversion efficiency γ_{SH} can be achieved via increase of efficiency of the coupling between the pump beam and nanoresonator mode and, independently, by enlarging the nanodisk Q factor. On the other hand, when considering structures supporting optical resonances at both SH and pump frequencies, spectral and spatial mode overlap play an important role [16]. While spectral overlap can be improved by tuning pump and SH frequencies to coincide with some of the nanodisk eigenfrequencies, spatial overlap involves the mode matching of pump and induced SH polarization fields.

We start our study from the eigenmode analysis. We apply the resonant-state expansion (RSE) method [20] for the AlGaAs resonator with a fixed permittivity $\varepsilon = 10.73$, which corresponds to material dispersion at pump wavelength $\lambda = 1550$ nm (see Supplemental Material [21] for details). We choose the z direction as the disk axis and numerate modes by radial index, azimuthal index, n, and parity $p = 0, 1$ with respect to up-down reflection symmetry. Importantly, for different values of p and n the RSE analysis is performed independently and eigenmodes (resonant states) with $n = 0$ are rigorously divided into TE ($\mathbf{E} = E\mathbf{e}_\varphi$) and TM ($\mathbf{H} = H\mathbf{e}_\varphi$) types [28]. The spectrum of the resonant states of AlGaAs nanodisk with respect to disk aspect ratio r/h for even ($p = 0$) modes with $n = 0$ (TE polarization) and $n = 1$ is shown in Fig. 2(a) with blue and pink lines, respectively. The RSE method is truncated by $M = 16$, $N = 452$ for $n = 0$ modes and by $M = 16$, $N = 896$ for $n = 1$ modes. Here N is the number of basis modes with frequencies ω_i lying inside a circle of radius $|\omega_i R/c| \leq M$, where R is the radius of a sphere enclosing the nanodisk.

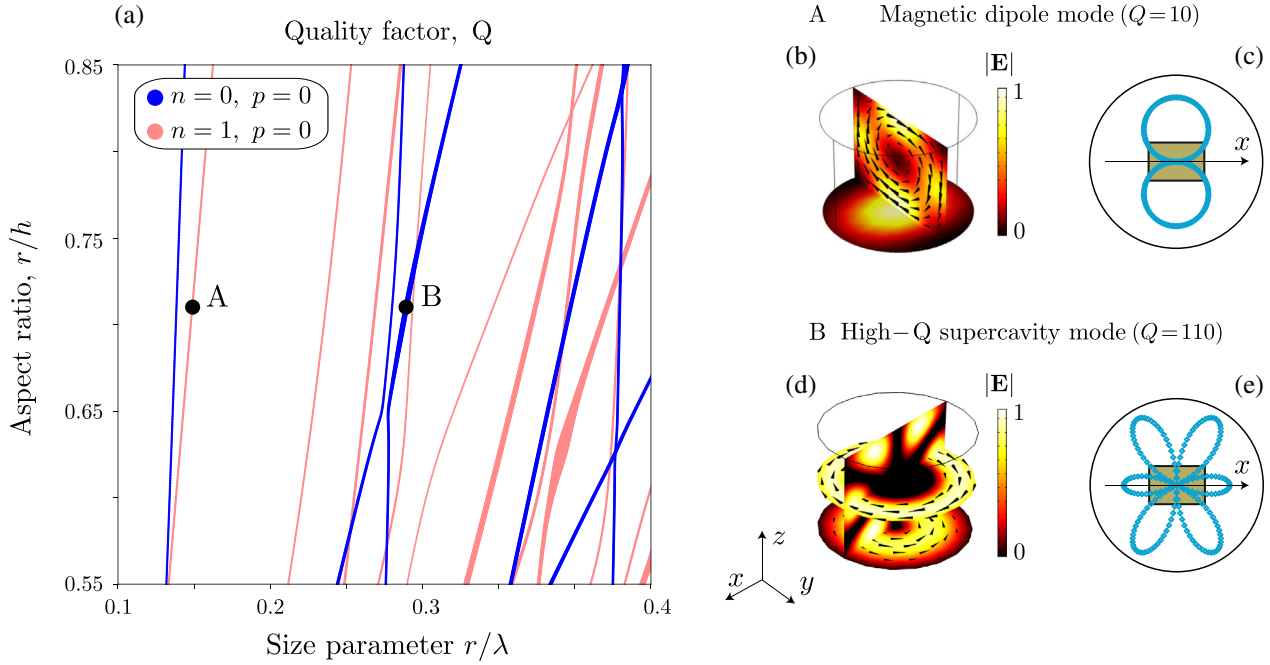

FIG. 2. Eigenmode spectra and electric field patterns for the AlGaAs nanodisk resonator. (a) Eigenfrequencies vs aspect ratio r/h for even ($p = 0$) modes with $n = 0$ and $n = 1$ shown with (blue and pink) lines, respectively; and linewidths are proportional to the Q factors of the modes. (b),(d) Electric field amplitude and (c),(e) directivity pattern of the MD and BIC-inspired modes, respectively.

As follows from Fig. 2(a), the spectrum evolution with respect to aspect ratio reveals a number of avoided resonance crossings describing strong mode coupling with the formation of high-Q states [3], which are the hallmark of non-Hermitian systems with both internal and external mode couplings [29]. Here, we focus on two resonant states of the nanodisk, marked as A and B in Fig. 2(a). The resonant state A with $p = 0$, $n = 1$ represents a conventional magnetic dipole (MD) mode with magnetic moment oriented transversely to the z direction. The resonant state B, with TE polarization and $p = 0$, $n = 0$, is a high-Q supercavity mode with $Q = 110$ associated with the BIC conditions. The electric field and directivity pattern of the MD and BIC modes are shown in Figs. 2(b)–2(e), respectively. The electric field of the BIC mode is uniform with respect to the azimuthal direction which allows us to achieve good mode matching with an azimuthally polarized pump and, according to Eq. (2), to increase the coupling efficiency η of the pump into the nanodisk compared to a linearly polarized pump [30].

To investigate the SHG response of the AlGaAs nanoresonator, we use three-dimensional electromagnetic simulations implemented with the finite-element method in COMSOL. The nanodisk is suspended in a homogenous background with refractive index 1. The dispersion of the AlGaAs permittivity is fitted from measured values [31], with losses taken into account. The nonlinear optical response from the material is estimated in the undepleted pump approximation. Thus, we use two subsequent simulations: as the first step, the linear optical response of the nanodisk excited at FF is evaluated, while, at the second step, we reproduce SHG by excitation of the nanodisk with the nonlinear currents induced by the FF beam. The induced second-order nonlinear polarizabilities, $P_i^{(2\omega)}$, are deduced from the electric fields in the resonator obtained in the first simulation step (at FF) using the $\chi^{(2)}$ tensor related to a material with the zincblende crystalline structure,

$$P_i^{(2\omega)} = \varepsilon_0 \chi_{ijk}^{(2)} E_j^{(\omega)} E_k^{(\omega)}, \qquad i \neq j \neq k, \tag{3}$$

where i, j, and k stand for the x, y, or z axes. For AlGaAs, we use $\chi_{ijk}^{(2)} = 100$ pm/V [32]. Subsequently, we explore two different scenarios. First, we use a focused linearly polarized Gaussian beam with a 60° angle of incidence with respect to the disk base. Second, observing the magnetic nature of the BIC resonance, we use a focused azimuthally polarized beam [30] to enhance selectively optical coupling from the pump beam. The estimated ρ_{SH} for all the analyzed scenarios are listed in Table I. As can be seen, the BIC-driven intrinsic SHG conversion efficiency achieves values as high as 2×10^{-2} W^{-1}, regardless of the pump beam polarization. As expected, η is higher for the azimuthally polarized pump than for the linearly polarized one due to the symmetry of the electric field of the supercavity mode shown in Fig. 2(d). This means that for the same incident power on the nanodisk cross section, using an azimuthally polarized beam results in an increase of about a factor of 100 in the generated SH power P_{SH}.

TABLE I. Enhancement of the SH response using different combinations of modes at the fundamental frequency and optical excitations. The columns from left to right report the mode description at the FF, the polarization of the electric filed in the pump beam at the FF, intrinsic SH conversion efficiency ρ_{SH} defined in Eq. (1), the coupling coefficient η, the wavelength corresponding to the FF, and the resonance Q factor.

FF mode	Polarization	$\rho_{SH} \times 10^4$ (W^{-1})	η	λ_{FF} (μm)	Q factor
BIC	Azimuthal	210	0.77	1.55	110
BIC	Linear	270	0.06	1.55	110
MD	Linear	1.8	0.84	2.98	10

As a reference, we compare the enhancement of the BIC-driven SH nonlinear response to that achieved by using the MD resonance at FF, for which many examples in the literature report a very high efficiency (see, e.g., Refs. [33,34]). Since the observed nonlinear phenomena are volumetric effects, for a fair comparison we kept the disk volume constant. The results from the numeric SHG experiments using the MD mode as FF are summarized in the last row of Table I. As can be seen, the estimated SH conversion efficiency is of the same order of magnitude compared to previous works, see, e.g., Ref. [16], but is smaller by a factor of 100 than that achieved by using the BIC mode at FF. Such an enhancement can be ascribed to the increase of the Q factor of the mode at FF, that is shown in the last column of Table I. As expected for second-order nonlinear phenomena, their intensities scale approximately with the factor $(Q/V)^2$, where we use the nanoscale definition of the mode volume V [35]. In our case, since the resonator volume is constant while the mode Q factor increases by a factor of 10 from MD to BIC regime, a rough estimate would indeed suggests that a 100-fold improvement of the second-order nonlinear interaction should be expected, as found in our numerical simulations.

To understand the SHG enhancement driven by the BIC-inspired supercavity mode, we analyze the value of ρ_{SH} as a function of the nanodisk aspect ratio by tuning the FF mode on and off the BIC condition. These calculations are performed at a fixed pump wavelength to move exactly along the dispersion line for the mode that is calculated and shown in Fig. 2(a). The results depicted in Fig. 3 (with red solid curve) show that ρ_{SH} reaches its highest value in the region corresponding to the BIC mode condition. The dependence of ρ_{SH} on the nanodisk aspect ratio is, from one side, due to the scaling of the Q factor at FF and, from the other side, due to the resonant response at the SH frequency. Indeed, the insets

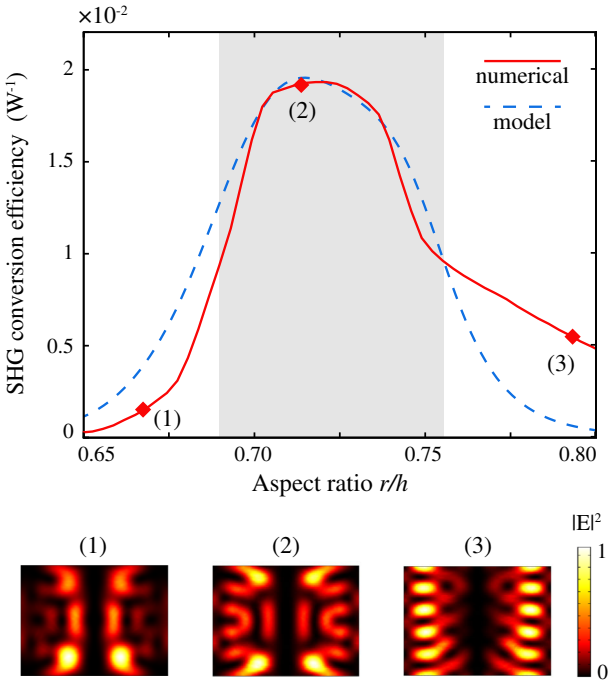

FIG. 3. SHG conversion efficiency ρ_{SH} as a function of the nanoparticle aspect ratio r/h calculated by nonlinear simulations in COMSOL (red solid line) and analytically from the model [Eq. (4)] (blue dashed line). Gray area represents the full-width at half-maximum band of the calculated SHG conversion efficiency. Lower insets: Intensity maps at the SH field in a longitudinal nanodisk cross section for the aspect ratios of 0.675 (1), 0.71 (2), and 0.79 (3).

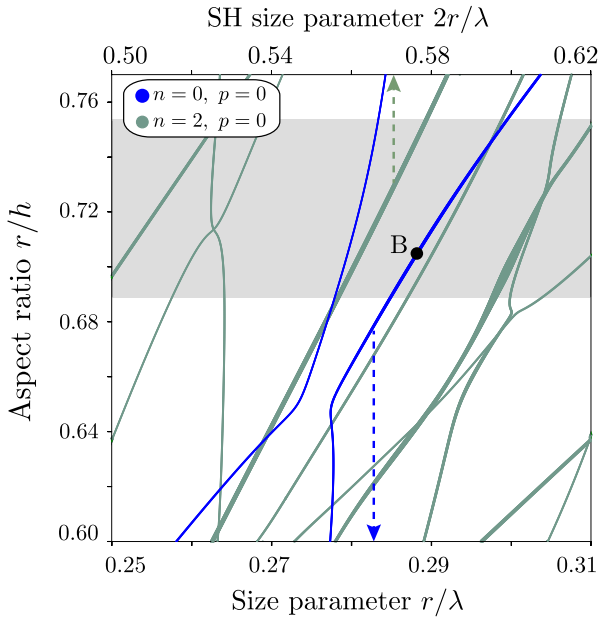

FIG. 4. Eigenfrequencies dependence on disk aspect ratio r/h for the FF modes with the indices $p = 0, n = 0$ (TE) and SH modes with $p = 0, n = 2$ are shown with blue and cyan lines, respectively. The supercavity mode is marked with B as in Fig. 2(a). Dot sizes are proportional to the mode Q factor. Pump and SH frequencies are shown in lower and upper horizontal scale, respectively.

in Fig. 3 show that the field profile of the SH response evolves with respect to r/h.

To illustrate further this phenomenon, we analyze the coupling between the induced SH polarization and nanodisk eigenmodes applying the RSE at the SH frequency. The electric field of the BIC mode has only one nonzero component $E_{\varphi}^{(\omega)}$, which does not depend on the azimuthal angle exhibiting even symmetry with respect to up-down reflection, thus $E_i(r,\phi,z) = -E_i(r,\phi+\pi,z)$ with $i = x, y$. From Eq. (3) and the BIC mode symmetry, it follows that only resonant states of the nanodisk with the indices $p = 0$ and $n = 2$ are excited at the SH frequency.

Figure 4 shows the evolution of the nanodisk eigenmode spectrum with respect to the aspect ratio for modes with $p = 0$, $n = 0$ (TE) and $p = 0$, $n = 2$ calculated by means of the RSE approach. As n Fig. 2, we perform all calculations for the pump wavelength of 1550 nm. The range of aspect ratios for which the calculated SHG conversion efficiency is higher than the half-maximum of all calculated values (see Fig. 3) is shown by a gray shadow in Fig. 4. Perfect spectral matching between the modes occurs when two classes of curves overlap. Figure 4 shows that there is only one resonant state at SH frequencies that can be excited by the pump in the vicinity of the supercavity mode.

Thus, we apply the temporal coupled mode theory (see Supplemental Material [21]) to estimate the SHG efficiency as a function of the pump frequency ω

$$\tilde{\rho}_{SH} = C\left[\frac{\gamma_{SH}}{(2\omega-\omega_{SH})^2+\gamma_{SH}^2}\right]\left[\frac{\gamma_{FF}}{(\omega-\omega_{FF})^2+\gamma_{FF}^2}\right]^2, \quad (4)$$

where C is a normalization constant, ω_{FF}, γ_{FF}, ω_{SH}, and γ_{SH} are the FF and SH resonant frequencies and decay rates, respectively. The calculation of $\tilde{\rho}_{SH}$ for resonant conditions $\omega = \omega_{FF}$ is superimposed onto the simulation results in Fig. 3, where we observe a good agreement between the two results.

In addition, we also notice that the intensity-dependent nonlinearity can change the position of the BIC resonances [36,37], and thus provides an efficient tuning of the high-Q states.

In conclusion, we have presented a new strategy to increase substantially nonlinear response at the nanoscale by employing the BIC concept. We have predicted that the SHG conversion efficiency in AlGaAs nanoantennas can be increased by at least 2 orders of magnitude compared to earlier results, due to the mode structure engineering. The value of γ_{SH} is comparable to state-of-the-art on-chip scale whispering gallery mode resonators with a small (16–25 μm^2) device footprint [38,39]. These results show the great potential of Mie-resonant semiconductor nanostructures for nonlinear nanophotonics, and they constitute a significant step towards the development of highly efficient frequency conversion metadevices.

The authors acknowledge financial support from the Australian Research Council, the Russian Science Foundation (17-12-01581), and also the Erasmus Mundus NANOPHI project, Contract No. 2013 5659/002-001. K. K. acknowledges the Foundation for the Advancement of Theoretical Physics and Mathematics BASIS for the valuable financial support. Y. K. thanks Albert Polman, Anatoly Zayats, Andrey Bogdanov, Bo Zhen, Harry Atwater, Marin Soljačić, Mikhail Rybin, Sergey Kruk, and Yuen-Ron Shen for useful discussions and suggestions.

[1] S. S. Kruk and Y. S. Kivshar, ACS Photonics **4**, 2638 (2017).
[2] A. I. Kuznetsov, A. E. Miroshnichenko, M. Brongersma, Y. S. Kivshar, and B. Lukýanchuk, Science **354**, aag2472 (2016).
[3] M. V. Rybin, K. L. Koshelev, Z. F. Sadrieva, K. B. Samusev, A. A. Bogdanov, M. F. Limonov, and Y. S. Kivshar, Phys. Rev. Lett. **119**, 243901 (2017).
[4] C. W. Hsu, B. Zhen, A. D. Stone, J. D. Joannopoulos, and M. Soljačić, Nat. Rev. Mater. **1**, 16048 (2016).
[5] H. Friedrich and D. Wintgen, Phys. Rev. A **32**, 3231 (1985).
[6] A. F. Sadreev, E. N. Bulgakov, and I. Rotter, Phys. Rev. B **73**, 235342 (2006).
[7] C. W. Hsu, B. Zhen, J. Lee, S. L. Chua, S. G. Johnson, J. D. Joannopoulos, and M. Soljačić, Nature (London) **499**, 188 (2013).
[8] F. Monticone and A. Alú, Phys. Rev. Lett **112**, 213903 (2014).
[9] M. Rybin and Y. Kivshar, Nature (London) **541**, 164 (2017).
[10] M. Kauranen and A. V. Zayats, Nat. Photonics **6**, 737 (2012).
[11] D. Smirnova and Y. S. Kivshar, Optica **3**, 1241 (2016).
[12] M. Kauranen, Science **342**, 1182 (2013).
[13] J. Butet, P.-F. Brevet, and O. J. F. Martin, ACS Nano **9**, 10545 (2015).
[14] M. Celebrano, X. Wu, M. Baselli, S. Gromann, P. Biagioni, A. Locatelli, C. De Angelis, G. Cerullo, R. Osellame, B. Hecht, L. Duó, F. Ciccacci, and M. Finazzi, Nat. Nanotechnol. **10**, 412 (2015).
[15] X. Y. Z. Xiong, L. J. Jiang, E. I. Wei, Y. H. Lo, M. Fang, W. C. Chew, and W. C. Choy, Phys. Rev. A **94**, 053825 (2016).
[16] L. Carletti, A. Locatelli, O. Stepanenko, G. Leo, and C. De Angelis, Opt. Express **23**, 26544 (2015).
[17] S. Liu, M. B. Sinclair, S. Saravi, G. A. Keler, Y. Yang, J. Reno, F. Setzpfandt, I. Stause, T. Pertsch, and I. Brener, Nano Lett. **16**, 5426 (2016).
[18] R. Camacho-Morales, M. Rahmani, S. Kruk, L. Wang, L. Xu, D. A. Smirnova, A. S. Solntsev, A. Miroshnichenko, H. H. Tan, F. Karouta, S. Naureen, K. Vora, L. Carletti, C. De Angelis, C. Jagadish, Y. S. Kivshar, and D. N. Neshev, Nano Lett. **16**, 7191 (2016).
[19] L. Ghirardini, L. Carletti, V. Gili, G. Pellegrini, L. Du, M. Finazzi, D. Rocco, A. Locatelli, C. De Angelis, I. Favero, M. Ravaro, G. Leo, A. Lematre, and M. Celebrano, Opt. Lett. **42**, 559 (2017).
[20] M. B. Doost, W. Langbein, and E. A. Muljarov, Phys. Rev. A **90**, 013834 (2014).
[21] See Supplemental Material at http://link.aps.org/supplemental/10.1103/PhysRevLett.121.033903 for details on the resonant state expansion method for the cylindrical eigenvalue problem, the analytical estimation of the SHG generation efficiency using the temporal coupled-mode theory, and comparison of SHG efficiencies for BICs and whispering gallery modes, which includes Refs. [22–27].
[22] E. Muljarov, W. Langbein, and R. Zimmermann, Europhys. Lett. **92**, 50010 (2011).
[23] L. Brillouin, J. Phys. Radium **3**, 373 (1932).
[24] S. Fan, W. Suh, and J. Joannopoulos, J. Opt. Soc. Am. A **20**, 569 (2003).
[25] D. V. Strekalov, C. Marquardt, A. B. Matsko, H. G. Schwefel, and G. Leuchs, J. Opt. **18**, 123002 (2016).
[26] J. U. Furst, D. V. Strekalov, D. Elser, M. Lassen, U. L. Andersen, C. Marquardt, and G. Leuchs, Phys. Rev. Lett. **104**, 153901 (2010).
[27] X. Guo, C.-L. Zou, and H. X. Tang, Optica **3**, 1126 (2016).
[28] J. A. Stratton, *Electromagnetic Theory* (John Wiley & Sons, New York, 2007).
[29] H. Cao and J. Wiersig, Rev. Mod. Phys. **87**, 61 (2015).
[30] T. Das, P. P. Iyer, R. A. DeCrescent, and J. A. Schuller, Phys. Rev. B **92**, 241110(R) (2015).
[31] S. Gehrsitz, F. K. Reinhart, C. Gourgon, N. Herres, A. Vonlanthen, and H. Sigg, J. Appl. Phys. **87**, 7825 (2000).
[32] V. F. Gili, L. Carletti, A. Locatelli, D. Rocco, M. Finazzi, L. Ghirardini, I. Favero, C. Gomez, A. Lematre, M. Celebrano, C. De Angelis, and G. Leo, Opt. Express **24**, 15965 (2016).
[33] E. V. Melik-Gaykazyan, S. S. Kruk, R. Camacho-Morales, L. Xu, M. Rahmani, K. Z. Kamali, A. Lamprianidis, A. E. Miroshnichenko, A. A. Fedyanin, D. N. Neshev, and Y. S. Kivshar, ACS Photonics **5**, 728 (2017).
[34] L. Carletti, D. Rocco, A. Locatelli, C. De Angelis, V. F. Gili, M. Ravaro, I. Favero, G. Leo, M. Finazzi, L. Ghirardini, M. Celebrano, G. Marino, and A. V. Zayats, Nanotechnology **28**, 114005 (2017).
[35] M. Notomi, Proc. IEEE **99**, 1768 (2011).
[36] E. N. Bulgakov and A. F. Sadreev, Phys. Rev. B **80**, 115308 (2009).
[37] S. D. Krasikov, A. A. Bogdanov, and I. V. Iorsh, Phys. Rev. B **97**, 224309 (2018).
[38] P. S. Kuo, J. Bravo-Abad, and G. S. Solomon, Nat. Commun. **5**, 3109 (2014).
[39] S. Mariani, A. Andronico, A. Lematre, I. Favero, S. Ducci, and G. Leo, Opt. Lett. **39**, 3062 (2014).